Article

Cd²⁺ Detection by an Electrochemical Electrode Based on MWCNT−Orange Peel Activated Carbon

Luis C. Beas-Bernuy, Andy A. Cardenas-Riojas, Sandy L. Calderon-Zavaleta, Ulises Quiroz-Aguinaga, Adolfo La Rosa-Toro, Elvis O. López, Yvan J. O. Asencios, Angelica M. Baena-Moncada,* and Golfer Muedas-Taipe*

Read Online

ACCESS | Metrics & More | Article Recommendations | SI Supporting Information

ABSTRACT: This study reports the development of a new electrochemical sensor based on a carbon paste electrode (CPE) composed of biomass-based orange peel activated carbon (ACOP) and multiwalled carbon nanotubes (MWCNTs), and this composite is used for the electrochemical detection of cadmium ions (Cd^{2+}). The ACOP/MWCNT composite was characterized by FTIR, Raman, and electrochemical impedance spectroscopy. The electrochemical evaluation of Cd^{2+} was performed using square wave and cyclic voltammetry. The ACOP/MWCNT−CPE electrochemical sensor exhibited a coefficient of determination r^2 of 0.9907, a limit of detection of 0.91 ± 0.79 μmol L^{-1}, and a limit of quantification of 3.00 ± 2.60 μmol L^{-1}. In addition, the developed sensor can selectively detect Cd^{2+} in the presence of different interferents such as Zn^{2+}, Pb^{2+}, Ni^{2+}, Co^{2+}, Cu^{2+}, and Fe^{2+} with a relative standard deviation (RSD) close to 100%, carried out in triplicate experiments. The ACOP/MWCNT−CPE presented high sensitivity, stability, and reproducibility and was successfully applied for the detection of Cd^{2+} in river water samples with recovery rate values ranging from 97.33 to 115.6%, demonstrating to be a very promising analytical alternative for the determination of cadmium ions in this matrix.
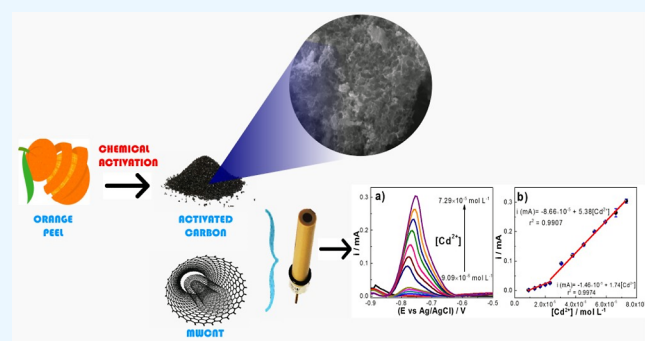
■ INTRODUCTION

Human beings suffer significant harm from environmental pollution caused by a variety of pollutants. Among these harmful substances are heavy metals (HMs).[1] A wide range of HMs are found in aquatic systems. These include Zn^{2+}, Cu^{2+}, Fe^{2+}, Mn^{2+}, Cd^{2+}, Hg^{2+}, Pb^{2+}, and As^{3+}. The presence of these HMs is mainly attributed to activities such as mining, automotive industry, and the discharge of agricultural and urban wastes.[2−4] The occurrence of these HMs is primarily attributed to activities such as mining, the automotive industry, and the release of agricultural and urban waste. These HMs, even in low concentrations, can accumulate within the body and interact with biological ligands containing elements like N, S, and O. This interaction leads to severe health complications for the human body,[4,5] with the maximum allowable level of Cd^{2+} in water being 0.026 μmol L^{-1}.[6] Therefore, the accurate detection of trace amounts of Cd^{2+} in water holds significance, as cadmium ranks among the primary pollutants that detrimentally affect the environment. It is widely recognized as one of the most extremely toxic HMs, potentially giving rise to conditions such as anemia, hypertension, cancer, edema, arthritis, kidney and skeletal damage, etc.[7,8] As a result, diverse methodologies have been employed for the analysis of cadmium in water. Spectroscopic techniques such as atomic absorption spectrometry (AAS),[9] flame atomic absorption (FAAS),[10] X-ray fluorescence spectroscopy,[11] and single particle inductively coupled plasma mass spectrometry (SP-ICP-MS)[12] have been utilized for this purpose. However, these methods have limitations stemming from their high testing costs and time-consuming analysis procedures. On the flip side, electrochemical methods offer a contrasting advantage, being characterized by their affordability, swift sample analysis, user-friendly nature, reliability, and suitability for on-site applications. This category includes techniques like amperometry,[13] voltammetry,[14,15] and potentiometry,[16] all of which are employed for the precise detection of trace amounts of Cd^{2+}.[17]

Among the voltammetric approaches utilized for analyzing these HMs, square wave voltammetry (SWV) and differential pulse voltammetry (DPV) stand out as the most extensively employed. These techniques offer notable benefits, boasting remarkable selectivity, portability, cost-effectiveness, expedi-

tious analysis, and excellent sensitivity.[17] The efficiency of the electrochemical method depends largely on the electrode employed. The modification of the working electrode is generally used to improve the conductivity,[18] selectivity,[19] sensitivity,[20] stability,[19] and surface area[21] often involves the modification of the working electrode; consequently, research efforts have been directed toward developing electrochemical sensors based on novel carbonaceous materials that exhibit exceptional efficiency in detecting trace metal ions. An exemplary instance involves the widespread use of glassy carbon electrodes in electrochemical sensors due to their inherent surface stability.[22] Furthermore, these electrodes can be modified with different types of molecules,[23] nanostructures,[24] polymers,[25] and so on. Remarkable improvements in sensor sensitivity have been achieved, resulting in a range limit of detection (LOD) spanning from 0.0005 to 0.123 μmol L^{-1}.

Multiwalled carbon nanotubes (MWCNTs) exemplify carbonaceous materials that have been extensively investigated due to their diverse applications even though the synthesis process for MWCNT incurs a high cost.[26]

The cylindrical configuration of the MWCNT results in multiple concentric layers of graphene, presenting a distinctive arrangement of sp^2-hybridized carbon atoms in hexagonal structures. This configuration grants MWCNTs exceptional thermal and electrical conductivity and, for example, Sreekanth et al. 2021, carried out a study to detect cadmium using MWCNT, obtaining a LOD of 0.002 μmol L^{-1}.[27,28] On the other hand, activated carbons (ACs) derived from biomasses have gained traction in electroanalytical applications. AC-based electrochemical sensors are very promising due to their inherent structural characteristics, physicochemical properties, and high sensitivity. Academic researchers have also directed their efforts toward generating ACs from agricultural waste materials.[29,30] This practice not only augments economic returns but also diminishes contamination through attributes like extensive surface area, well-developed pore structures, rapid adsorption kinetics, and relatively straightforward regeneration procedures.[31]

Several biomass materials have been used, such as rice husk,[32] corn cob,[33] eucalyptus leaf,[34,35] fruit peel,[36] etc. To illustrate, the utilization of biomass waste like orange peel, (OP) for AC production, using various activating agents (KOH, NaOH, and H$_3$PO$_4$),[37−39] is commonplace. This versatile form of carbon has found applications in diverse studies encompassing dye and HM removal,[40−42] supercapacitors,[43] batteries,[44] and gas sensors.[45] Despite the comprehensive exploration of properties and applications pertaining to biomass-sample-derived carbon materials, unexplored avenues remain ripe for investigation. These materials have the potential to be harnessed in novel technologies that have not yet been widely explored, particularly in the field of electrochemical sensors.

For this reason, the present study utilizes AC derived from orange peel (ACOP) due to its notable attributes, including high sensitivity, low-cost, ecofriendliness, porosity, surface area, and the presence of active sites. The fabrication of this sensor rests upon a carbon paste electrode composed of ACOP and MWCNT, termed as ACOP/MWCNT−CPE. The incorporation of MWCNTs into ACOP serves to enhance both material conductivity and sensitivity, resulting in the formation of the ACOP/MWCNT composite. This strategy has been explored in previous research and stands as a pivotal aspect of this study.[29,46,47] The developed sensor demonstrates the

capability to precisely detect even trace concentrations of the Cd^{2+} metal ion in water. Moreover, the successful identification of cadmium ions in real water samples within the controlled laboratory environment was achieved through meticulous pH adjustments.

Through this methodology, we can establish effective monitoring and management of these pollutants within water bodies, which currently present significant environmental challenges. Furthermore, the potential scope of this material's application in forthcoming research extends to addressing other contaminants such as lead, mercury, zinc, and more.

■ EXPERIMENTAL SECTION

Reagents and Solutions. All solutions were freshly prepared using ultrapure water (resistivity ≥ 18.2 MΩ cm at 25 °C) obtained from a Milli-Q purification system (Millipore). Standard solution of 1000 mg L^{-1} of Cd^{2+}, iron salts K$_4$[Fe(CN)$_6$]·2H$_2$O/K$_3$[Fe(CN)$_6$] were obtained from Sigma-Aldrich. The Zn^{2+}, Pb^{2+}, Ni^{2+}, Co^{2+}, Cu^{2+}, and Fe^{2+} salts were used as interferences. Stock solutions of 1.0×10^{-2} mol L^{-1} of Cd^{2+} were prepared by dissolving in 0.1 mol L^{-1} HCl. Electrolyte solutions of 0.1 mol L^{-1} at H$_2$SO$_4$, HCl, H$_3$PO$_4$, acetate buffer, Britton Robinson buffer, phosphate buffer, KCl, NaCl, KOH, and acetic acid were also prepared for use as electrolytes. All reagents were obtained from Sigma-Aldrich and Merck.

Production of ACOP. Orange peels (OPs) were meticulously sliced into small pieces, washed several times with ultrapure water, and dried at 100 °C for 8 h. Then, 60 g of OP was mixed with a phosphoric acid solution (15 g of phosphoric acid in 100 mL of ultrapure water). The resultant mixture was then transferred into a stainless-steel autoclave and placed in a Teflon reactor and heated at 120 °C for 2 h. The resulting mixture was washed until reaching a pH of 7 and dried at 60 °C for 24 h. The solid obtained was mixed with 5 mol L^{-1} KOH at room temperature for 24 h, filtered, and dried for an additional 48 h at 60 °C. The ensuing material was then subjected to carbonization, a process executed within a tubular furnace under a continuous flow of nitrogen gas. This entailed a temperature ascent from 25 to 800 °C at a heating rate of 10 °C min^{-1}. The temperature was subsequently maintained at 800 °C for 4 h, after which it was allowed to cool gradually to room temperature. The culmination of this sequence yielded the sought-after carbon product.[42,48]

Preparation of ACOP/MWCNT Paste Electrode. To obtain the carbon paste electrode, 1 mL of 0.05 mol L^{-1} KCl was added and carefully mixed with 100 mg of ACOP/MWCNT at a ratio of 1:1 using a mortar and pestle and then dried at ∼50 °C for 15 min. A supplementary addition of 80 μL of mineral oil was executed to yield a paste consistency. Subsequently, the prepared paste was packed into the cavity of the electrode, having a diameter of 3 mm and a depth of 1.5 mm. The modified carbon paste electrode was named ACOP/MWCNT−CPE.
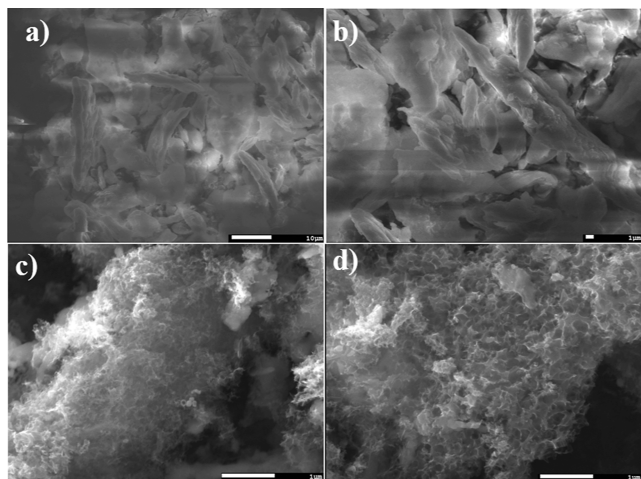
Characterization of the Developed Materials. *Physicochemical Evaluation of ACOP, MWCNT, and ACOP/MWCNT.* ACOP, MWCNT, and ACOP/MWCNT materials were investigated by physicochemical techniques such as Raman spectroscopy, performed using the XploRA model from Horiba Scientific, and IR spectroscopy, employing the Alpha-Bruker FT-IR spectrometer, facilitated an insightful vibrational analysis of the functional groups present within the materials.

Evaluation of the ACOP/MWCNT−CPE Sensor and the Electrochemical Detection of Cd^{2+}. Electrochemical assessments were conducted via cyclic voltammetry (CV), SWV, and electrochemical impedance spectroscopy (EIS). These measurements were executed using a potentiostat−galvanostat PGSTAT204 Autolab (Eco-Chemie, The Netherlands) using Nova software. A three-electrode configuration within a glass electrochemical cell was employed: the counter electrode comprised a graphite bar, the reference electrode was an Ag/AgCl electrode (3 mol L^{-1} KCl) as the reference electrode, and the working electrode was a carbon paste electrode composed of ACOP/MWCNT−CPE.

The electrochemical characterization of ACOP/MWCNT−CPE was performed at different electrolytes such as HCl, H_2SO_4, acetate buffer, Britton Robinson buffer, phosphate buffer, acetic acid, KCl, KOH, and NaCl, and in the presence of Cd^{2+} using 0.1 mol L^{-1} HCl solution by CV at a scan rate of 0.025 V s^{-1}. The SWV analyses were carried out with the following parameters: amplitude of 0.075 V, scan rate of 0.025 V s^{-1} and 30 s of conditioning time. EIS and CV analyses were recorded in a solution of the $[Fe(CN)_6]^{4-}/[Fe(CN)_6]^{3-}$ redox couple 5.0 mmol L^{-1} in an electrolyte of KCl 1 mol L^{-1} and employed a scan rate of 0.005 V s^{-1}. CV and SWV techniques were used to evaluate the stability, sensitivity, limits of detection (LOD), limits of quantification, and selectivity of the sensor in the presence of different interferents such as Zn^{2+}, Pb^{2+}, Ni^{2+}, Co^{2+}, Cu^{2+}, and Fe^{2+}, during the electrochemical detection of Cd^{2+}. Lastly, the optimized sensor's capability in determining Cd^{2+} concentrations in the Rímac River of Peru was verified, and the sensor's validity was substantiated via the atomic absorption spectroscopy technique.

■ RESULTS

Morphological and Physicochemical Evaluation of the ACOP, MWCNT, and ACOP/MWCNT. Morphological examination of the OP and ACOP materials is illustrated in Figures 1, S1, and S2. Figure 1a,b shows magnified views of the OP structure, revealing the absence of observable pores at this scale. Furthermore, Figure S1 presents an EDS analysis of the OP, indicating the presence of carbon (C) and oxygen (O) atoms with respective proportions of 64.4 and 35.4%. SEM images of ACOP (Figure 1c,d) distinctly illustrate the surface porosity at varying magnifications. Figure S2 (see the Supporting Information) provides the EDS analysis of ACOP, displaying an increase in the percentage of carbon atoms (C) within the range of 76.2 to 83.2%. This augmentation arises from the carbonization process that was undertaken. Oxygen atoms are also discernible at a proportion of 13.4 to 17.4%.[49]

Isotherms for OP and ACOP are shown in Figure S3a. Based on the figure, ACOP displays a mixed behavior, exhibiting characteristics of both type I and type II isotherms. At lower relative pressures ($P/P_0 < 0.35$), a type I behavior is evident, indicated by a gradual concave rise toward the pressure axis. However, at relative pressures higher than 0.35, a distinct shift toward a type II behavior is observed, with a steep initial rise as the relative pressure increases. The presence of a closed loop intercepted by $P/P_0 = 1$ on the adsorption−desorption curves confirms the limited presence of mesopores.[50,51] The predominant region is identified as type II, indicating the absence of micropores on the carbon surface.[50] Nevertheless, nitrogen adsorption occurs through the presence of macropores with a diameter of 80 nm, significantly contributing to the overall distribution.

Surface area calculations via the BET method yield a value of 128.28 m^2 g^{-1}, as evidenced in Figure S3a,b. On the contrary, unmodified OP displays an anticipated dearth of micropores on its surface, resulting in a small surface area of 0.38 m^2 g^{-1}.

Figure 2 shows the thermal gravimetric analysis (TGA) and XRD patterns of the starting material (OP) and the prepared material (ACOP). Within Figure 2a, a depiction of TGA elucidates the impact of the temperature on both OP and ACOP samples. During this analysis, the weight loss of the samples is observed as the temperature increases up to 800 °C. Within the OP material, the initial weight reduction, occurring between 50 and 150 °C (5% loss), is attributed to the inherent humidity content. Subsequently, a more substantial mass decline spanning 150 to 270 °C (35% loss) corresponds to the decomposition of cellulose, hemicellulose, and lignins.[52] Following this, a 30% weight decrease proceeds from 270 to 400 °C, signifying the ultimate decomposition of hemicellulose. The final phase involves complete sample carbonization, manifesting as a 7% weight reduction between 400 and 800 °C.[53,54] The total mass loss of the ACOP was 15%, signifying its successful carbonization at a temperature of 800 °C.[55] The XRD patterns for both the OP and ACOP materials are shown in Figure 2b. The ACOP spectrum shows two broad and small peaks at 26° and 43°, which are attributed to the (002) and (100/101) planes corresponding to the graphite structure. The absence of well-defined, robust peaks points to the amorphous nature characterizing the carbonaceous material.[56] Additionally, discernible peaks emerge at angles of 35° and 40°, aligning with (020) and (022) planes. This presence indicates a pronounced degree of graphitization within the carbon matrix, attesting to its structural transformation.[57,58]

Figure 3 illustrates the Raman and IR spectra of the carbonaceous materials. Raman spectroscopy is commonly employed to assess various properties of carbonaceous materials, including their degree of graphitization, hybridization, and carbon−carbon bond vibrations. The intensities of the G and D bands, quantified by the I_D/I_G ratio, offer valuable insights into these attributes, as depicted in Figure 3a and Table 1.[59,60]
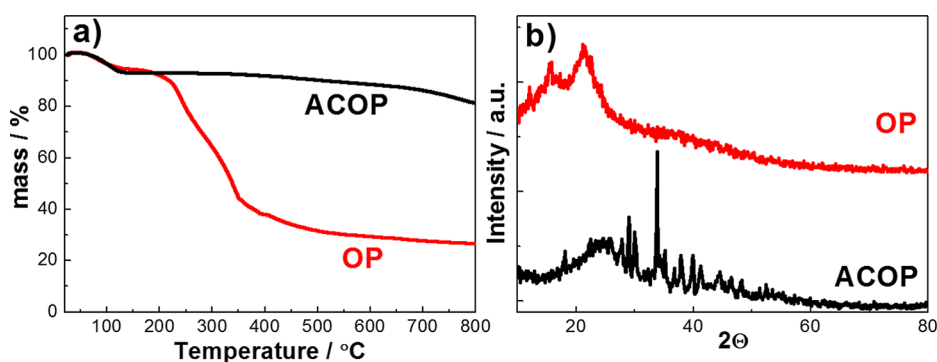

Figure 1. SEM images at different magnifications: (a,b) OP and (c,d) ACOP.

Figure 2. Analysis of the OP and ACOP materials by (a) TGA and (b) XRD pattern.
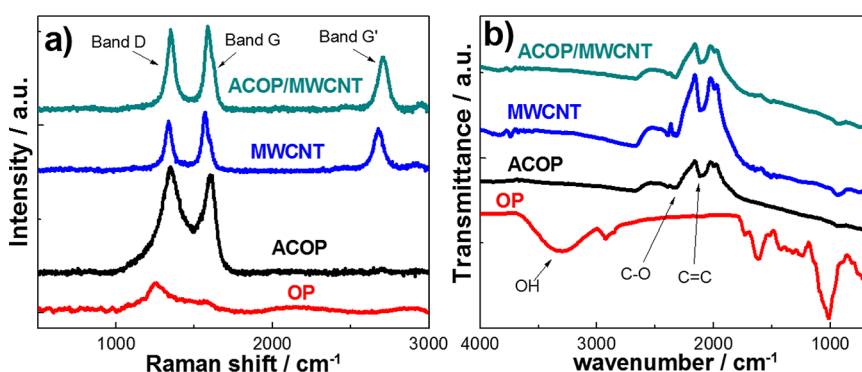

Figure 3. (a) Raman spectrum with a 532 nm laser and 10% power and (b) IR spectrum of the materials OP, ACOP, MWCNT, and ACOP/MWCNT.

Table 1. Values of the Intensities of Bands D and G of Carbonaceous Materials

|	intensity		ratio
carbon materials	I_D	I_G	I_D/I_G
OP	-	-	-
ACOP	255.3	220.1	1.16
MWCNT	138.5	175.4	0.79
ACOP/MWCNT	226.5	243	0.93

In the case of the OP material, discernible D and G bands are absent, a feature attributed to the typical absence of C=C bonds found in carbonaceous materials. Conversely, ACOP displays characteristic D (1352 cm^{-1}) and G (1602 cm^{-1}) bands associated with carbonaceous materials, accompanied by an I_D/I_G ratio of 1.16. This ratio surpassing unity signifies a notable prevalence of defects in ACOP.[61] Furthermore, the lack of a weak second-order G' band at 2690 cm^{-1} serves as an indicator of crystalline lattice perfection within the spherical carbon layer.[62−65] Concerning the MWCNT and ACOP/MWCNT materials, their I_D/I_G ratios are 0.79 and 0.93, respectively. These values imply a heightened degree of order

in these carbons, attributed to the MWCNT structure and reinforced by the well-defined G' band.[62−65]

Distinctive peaks in the OP and ACOP materials are depicted in Figure 3b (IR spectrum). The OP spectrum exhibits peaks at 3400, 2920, and 1060 cm^{-1}, corresponding to the stretching vibrations of −OH, −CH, and −CO groups, respectively. Additionally, peaks at 1520 and 1615 cm^{-1} arise from the stretching vibrations of aromatic ring stretch and C=C groups, respectively; signifying the presence of carboxylic acids, acetate groups, ketones, aldehydes, and aromatic rings (refer to Table 2). The presence of these functional groups are potentially attributed to the presence of lignin, cellulose, and hemicellulose.[66−68] The OP spectrum displays more peaks compared with ACOP, indicating a higher concentration of organic functional groups on the material surface. In contrast, the ACOP spectrum does not present the bands at 3400 and 2920 cm^{-1}. In addition, IR bands attributed to C=O, C−O, and C−H are observed (Table 2), confirming its identity as an AC material. Furthermore, in ACOP/MWCNT and MWCNT, a vibration of the C−H group is observed at 932 cm^{-1}, followed by a peak at 1610 cm^{-1}, corresponding to the vibration of C=C bonds, characteristic of aromatic groups

Table 2. Values of the Vibrations of the Functional Groups and Bonds Present in the Carbonaceous Materials

	vibration v (cm^{-1})					
carbon materials	−OH	−CH	−C−O	aromatic ring	C=C	−C=O
OP	3400	2920	1060	1520	1615	1743
ACOP	-	932	-	1519	1610	-
MWCNT	-	932	-	1519	1610	-
ACOP/MWCNT	-	932	-	1519	1610	-
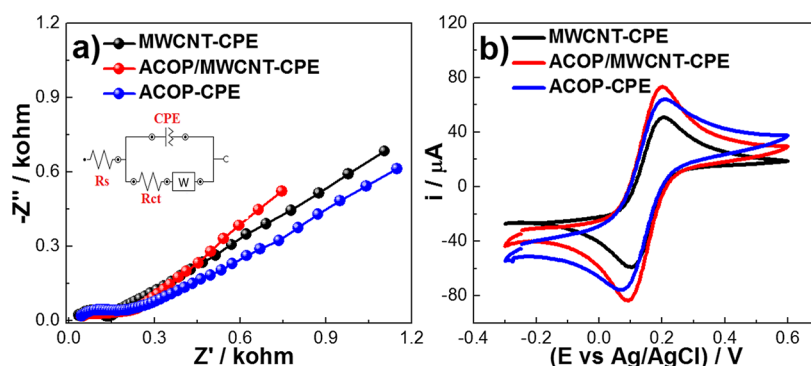
Figure 4. (a) Nyquist plot (OCP: 0.145 V), (b) CV at 0.005 V s^{-1} of ACOP−CPE, MWCNT−CPE, and ACOP/MWCNT−CPE in $[Fe(CN)_6]^{4-}/[Fe(CN)_6]^{3-}$ 5.0 mmol L^{-1} and KCl 1 mol L^{-1}.
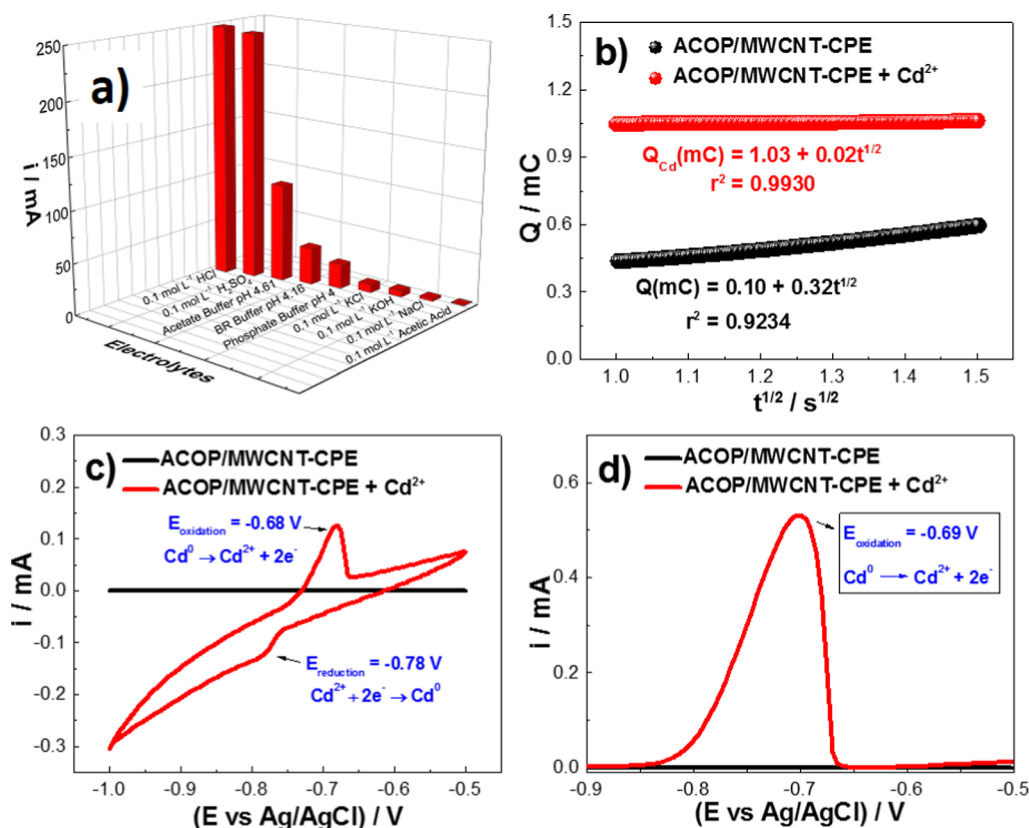

Figure 5. (a) Evaluation of Cd^{2+} in different electrolytes by SWV, (b) chronocoulometric analysis in the absence and in the presence of Cd^{2+} 9.0 × 10^{-4} mol L^{-1} at −0.7 V during 120 s, (c) CV at different scan rates at 0.025 V s^{-1} in the presence of Cd^{2+} 9.0 × 10^{-4} mol L^{-1}, and (d) evaluation of SWV in the presence and absence of Cd^{2+} 9.0 × 10^{-4} mol L^{-1} with the optimal parameters using the ACOP/MWCNT−CPE sensor in 0.1 mol L^{-1} HCl.

within the carbonaceous structure. Lastly, the absorption band at 1050 cm^{-1} indicates the asymmetric deformation vibrations of C−O molecules.[66−68]

Electrochemical Study of Carbon Materials. Figure 4a presents the EIS analysis utilizing a $[Fe(CN)_6]^{4-}/[Fe(CN)_6]^{3-}$ redox couple, a method employed to assess the electron transfer of this couple on the ACOP−CPE, MWCNT−CPE and ACOP/MWCNT−CPE surfaces. Additionally, this figure portrays the schematic equivalent circuit model, consisting of the electrolyte resistance (R_s) in series with the charge transfer resistance (R_{ct}), a Warburg impedance (W) and a constant phase element (CPE). These last three elements are connected in parallel, thus obtaining the Randles model. The values determined for the R_{ct} are 132.9, 137.7 and 103.7 Ω for

ACOP−CPE, MWCNT−CPE and ACOP/MWCNT−CPE, respectively. The decrease in R_{ct} is attributable to the presence of ACOP in the MWCNT, indicating the electron transfer enhancement between the ACOP/MWCNT−CPE sensor surface and the electrolyte solution. Figure 4b presents the CV of the evaluated electrodes in the $[Fe(CN)_6]^{4-}/[Fe(CN)_6]^{3-}$ redox couple, showing that the ACOP/MWCNT−CPE electrode exhibits heightened $[Fe(CN)_6]^{4-}/[Fe(CN)_6]^{3-}$ electron transfer on its surface, underscoring its capacity as a suitable sensor with substantial sensitivity for the electrochemical detection of Cd^{2+}.

Electrochemical Detection of Cd^{2+} by Means of the ACOP/MWCNT−CPE Sensor. In the context of the electrochemical detection of diverse pollutants, the selection of an
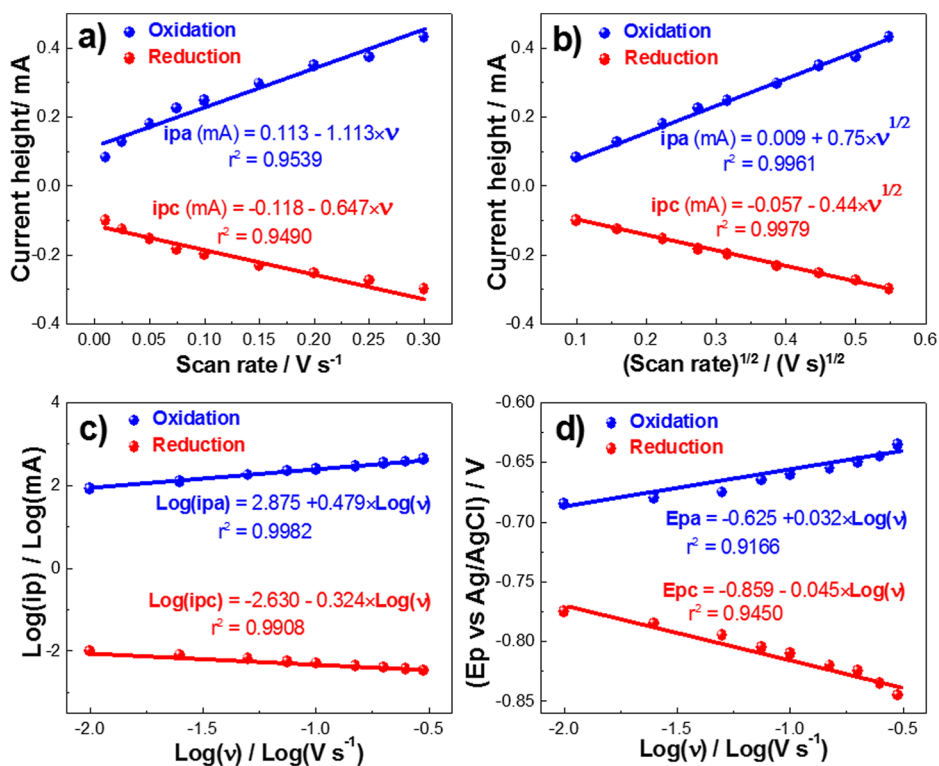
Figure 6. Study of ACOP/MWCNT−CPE at different scan rates 0.01−0.3 V s^{-1} in a HCl 0.1 mol L^{-1} Cd^{2+} 9.0 × 10^{-4} mol L^{-1}. The graphs show the relationship between (a) i_{pa} vs v, (b) i_{pa} vs $v^{1/2}$, (c) $\log(i_{pa})$ vs $\log(v)$, and (d) E_p vs $\log(v)$.

appropriate electrolyte solution holds significance. This choice impacts the attainment of an optimal electrochemical signal, specifically one that manifests a redox reaction (oxidation−reduction). In this vein, various electrolytes were examined for the detection of Cd^{2+} 9.0 × 10^{-4} mol L^{-1} using the ACOP/MWCNT−CPE sensor via the SWV electrochemical technique.

Figure 5a presents the oxidation current heights of Cd^{2+} using different electrolytes (HCl, H$_2$SO$_4$, acetate buffer, BR buffer, phosphate buffer, acetic acid, KCl, KOH, and NaCl). Notably, the optimal electrolyte was discerned at 0.1 mol L^{-1} HCl, as it yielded the highest signal. Consequently, subsequent assessments were conducted using this electrolyte.

For establishing the alteration in charge on the ACOP/MWCNT−CPE sensor's surface attributed to Cd^{2+} species, Anson's eq S1 (see the Supporting Information) was used. In this framework, the charge on the unmodified surface of the ACOP/MWCNT−CPE electrode is 0.1 mC. Upon the introduction of Cd^{2+} ions, an adsorbed charge of 1.03 mC is obtained (Figure 5b).[69] This indicates the presence of the Cd^{2+} detected by the developed sensor, and this is due to the electrostatic interaction between the carbonaceous structure's aromatic rings and its inherent functional groups with the Cd^{2+} ions; additionally, the porous structure of the carbonaceous material facilitates the adsorption of Cd^{2+} onto its surface (Figure 2a,b).[70]

Figure 5c portrays the discernible peaks corresponding to the redox reaction of 9.0 × 10^{-4} mol L^{-1} Cd^{2+} assessed through the ACOP/MWCNT−CPE sensor using the CV electrochemical technique within a 0.1 mol L^{-1} HCl medium at a scan rate of 0.025 V s^{-1}. The depicted peaks underscore the oxidation of Cd^0 to Cd^{2+} transpiring at −0.68 V and the reverse reduction of Cd^{2+} to Cd^0 occurring at −0.70 V.

$$Cd^0 \rightleftarrows Cd^{2+} + 2e^-$$

Figure 5d shows the SWV analysis conducted both in the absence and in the presence of at concentration of Cd^{2+} 9.0 × 10^{-4} mol L^{-1}. The SWV analysis reveals the oxidation peak corresponding to the conversion of Cd^0 to Cd^{2+}. In order to heighten the sensitivity of Cd^{2+} detection utilizing the ACOP/MWCNT−CPE sensor, the SWV parameters were optimized, yielding the following values: amplitude (E_{amp}) = 100 mV, step potential (E_{step}) = 1 mV, frequency (f) = 10 Hz, deposition potential (E_{dep}) = −0.7 V, deposition time (t_{dep}) = 120 s, conditioning potential (E_{ac}) = −0.8 V, and conditioning time (t_{ac}) = 120 s. These results are shown in Figure S4 (see the Supporting Information).

The electrochemical evaluation of Cd^{2+} was conducted in 0.1 mol L^{-1} HCl, and the results are presented in Figure S5 (refer to the Supporting Information section). The figure illustrates the CV of Cd^{2+} at various scan rates ranging from 0.025 to 0.3 V s^{-1}. The graph reveals the oxidation and reduction potentials of Cd^{2+}, with the oxidation occurring at −0.65 V and the reduction occurring at −0.81 V. Additionally, as the scan rate (v) increases, the current heights of both oxidation and reduction processes also increase proportionally. Furthermore, with an increase in the scan rate, there is a noticeable shift toward more positive potentials. It is noteworthy that there is a linear correlation between the scan rate (ranging from 0.01 to 0.3 V s^{-1}) and both the oxidation current peak (i_{pa}) and the reduction current peak (i_{pc}). In essence, as the scan rate rises, both the oxidation and reduction current peaks consistently intensify.

Figure 6 illustrates a set of distinct linear correlations involving various variables, including i_p vs v, i_p vs $v^{1/2}$, $\log(i_{pa})$ vs $\log(v)$, and E_p vs $\log(v)$, obtained at various scan rates. These associations, coupled with their corresponding current
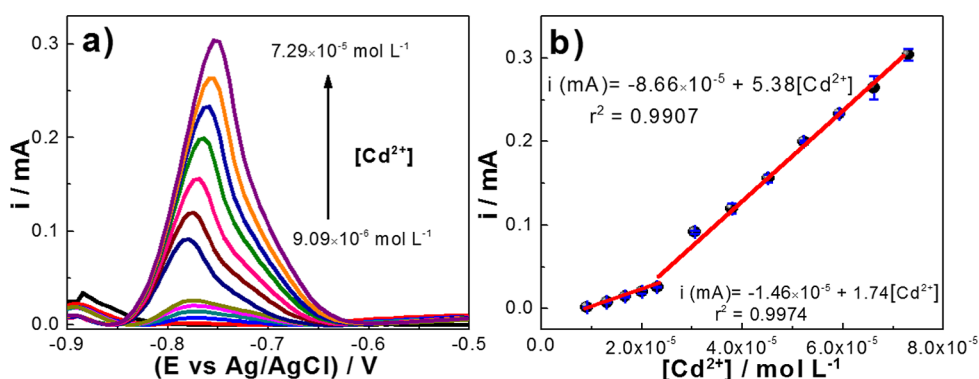
Figure 7. (a) SWV analysis of the ACOP/MWCNT−CPE sensor in the presence of Cd^{2+} at different concentrations in 0.1 mol L^{-1} HCl and (b) calibration curve of the anodic current heights as a function of Cd^{2+} concentrations.

heights, offer valuable insights into the electrochemical behavior of Cd^{2+} as assessed through the ACOP/MWCNT−CPE sensor.

In Figure 6a, the relationship between i_{pa} and i_{pc} demonstrates a high degree of linearity with an r^2 value close to 1.0. This suggests that the process is primarily dictated by the adsorption of cadmium onto the sensor surface. Similarly, Figure 6b displays the linear correlation between i_p and $v^{1/2}$, with high linearity (r^2 = 0.9961 and 0.9979). This indicates that the Cd^{2+} mechanism is controlled by the diffusion process on the sensor surface.

Figure 6c presents the linear relationship of $\log(I_{pa})$ vs $\log(v)$, indicating that the redox process associated with Cd^{2+} detection is governed by diffusion−adsorption. The high linearity observed (r^2 close to 1) further supports this inference. Lastly, Figure 6d illustrates the plot of E_p vs $\log(v)$, showing a satisfactory linear relationship. This graphic facilitates the determination of the number of electrons transferred in the redox reaction of Cd^{2+},[71,72] as described in the following equation

$$|E_p - E_{1/2}| = \frac{47.7}{\alpha \cdot n} (mV), \text{ (at 298 K)}$$

These findings, referenced from the study by Ascencio-Flores et al. in 2023,[71] suggest that the electrochemical process for Cd^{2+} is irreversible. Consequently, the number of transferred electrons (n) can be calculated by using the aforementioned equation. In this study the obtained n values is 2.38∼2 transferred in the cadmium reaction

This number of electrons are corroborated with the oxidation and reduction reaction of Cd^0 to Cd^{2+}/ Cd^{2+} to Cd^0.

Calibration Curve and Detection Limit for Determination of Cd^{2+}. The electrochemical detection of Cd^{2+} using the ACOP/MWCNT−CPE sensor was investigated through SWV in 0.1 mol L^{-1} of HCl under optimized experimental conditions. The results, depicted in Figure 7a, demonstrate that the current height increases proportionally with the addition of the Cd^{2+}. Figure 7b presents the resulting calibration curve, i_p vs $[Cd^{2+}]$, for the detection of Cd^2 This curve exhibits a notably correlation coefficient of r^2 = 0.9907. The LOD of the sensor is determined to be 0.91 ± 0.79 μmol L^{-1}, with a detection range of 7.29×10^{-5} to 9.09×10^{-6} mol L^{-1}. These measurements were performed in triplicate to ensure reliability. A comparative assessment of the LOD achieved by our developed sensor in relation to previous studies (as presented in Table 3) underscores that the ACOP/MWCNT−CPE sensor effectively falls within the established

working ranges and adheres to the maximum permissible limits.[73−75]

Table 3. Comparison of Different Modifications of Working Electrodes Based on Carbon for Cd^{2+} Detection[a]

electrode	technique	linear range and LOD (μmol L^{-1})	reference
Au-(Cys)PW	SWV	0.01−0.20, 0.009	76
nano-PPCPE/CPE	DPV	0.10−0.30, 0.078	21
poly(BPE)/g-C_3N_4/CPE	DPV	0.12−7.02, 0.080	77
Bi@BAC/CPE	DPV	0.50−50.0, 0.080	78
nZVI-BPC/GCE	SWV	2.00−50.0, 0.192	79
G/HNFQ-CPE	SWV	0.47−93.8, 0.21	80
ACOP/MWCNT−CPE	SWV	9.09−72.9, 0.910	this work

[a]NPC: N-(4-((4-((5-oxo-5H-benzo[a]phenoxazin-6-yl)amino)-phenyl)sulfonyl)phenyl)furan-2-carboxamide. Au-(Cys)PW: L-Cysteine tungstophosphate-modified polycrystalline gold electrode. PPCPE: Nanoporous pseudo carbon paste electrode. Poly(BPE)/g-C_3N_4: poly(2,5-bis(3,4-ethylenedioxythienyl)pyridine)/graphitic carbon nitride. Bi@BAC: Novel lotus root-like three-dimensional (3D) bismuth/biomass derived AC. nZVI-BPC: biomass-derived porous carbon along with nanoscale zerovalent iron. G/HNFQ-CPE: graphite (G) decorated with 2-hydroxy-1,4-naphthoquinone (HNFQ) incorporated in a carbon paste electrode (CPE).

ACOP/MWCNT−CPE Sensor Repeatability and Selectivity. Figure 8a demonstrates the repeatability of the ACOP/MWCNT−CPE sensor when subjected to Cd^{2+} ions, with a relative standard deviation (RSD %) of 2.68%. This low RSD % value suggests that the developed sensor exhibits sufficient repeatability.

To assess the selectivity of the proposed sensor, a selectivity analysis was performed in the presence of interferents including Zn^{2+}, Pb^{2+}, Ni^{2+}, Co^{2+}, Cu^{2+}, and Fe^{2+} at a concentration of 1×10^{-4} mol L^{-1}. These interferents were tested in a solution containing 4.75×10^{-4} mol L^{-1} of Cd^{2+} in 0.1 mol L^{-1} HCl. The variation percentage is depicted in Figure 8b. Notably, the electrochemical signals obtained in the presence of the interferents are similar to those of the Cd^{2+} signal. This demonstrates that the ACOP/MWCNT−CPE sensor can successfully detect Cd^{2+} ions even in the presence of the aforementioned interferents.

Validation of the Electrochemical Method by Atomic Absorption Spectroscopy. The validation of the ACOP/MWCNT−CPE sensor was carried out using atomic absorption analysis (AA) as a comparative method for
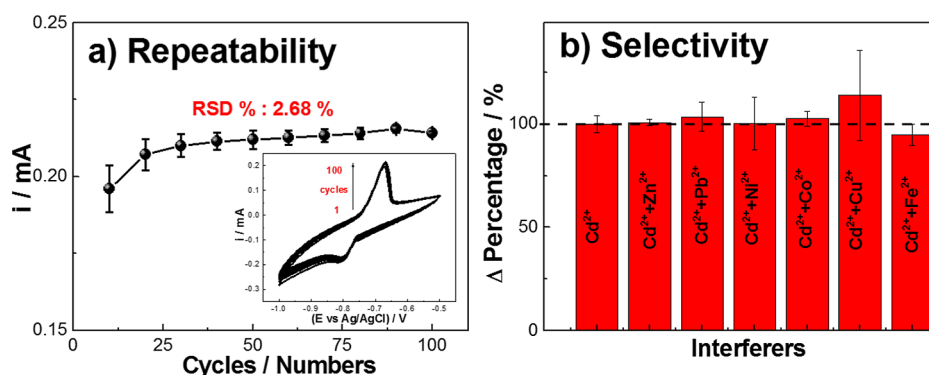
Figure 8. (a) Repeatability (insert: CV) and (b) selectivity evaluated by SWV in the presence of Cd^{2+} and different HMs evaluated by the ACOP/MWCNT−CPE sensor in the electrolyte 0.1 mol L^{-1} HCl.
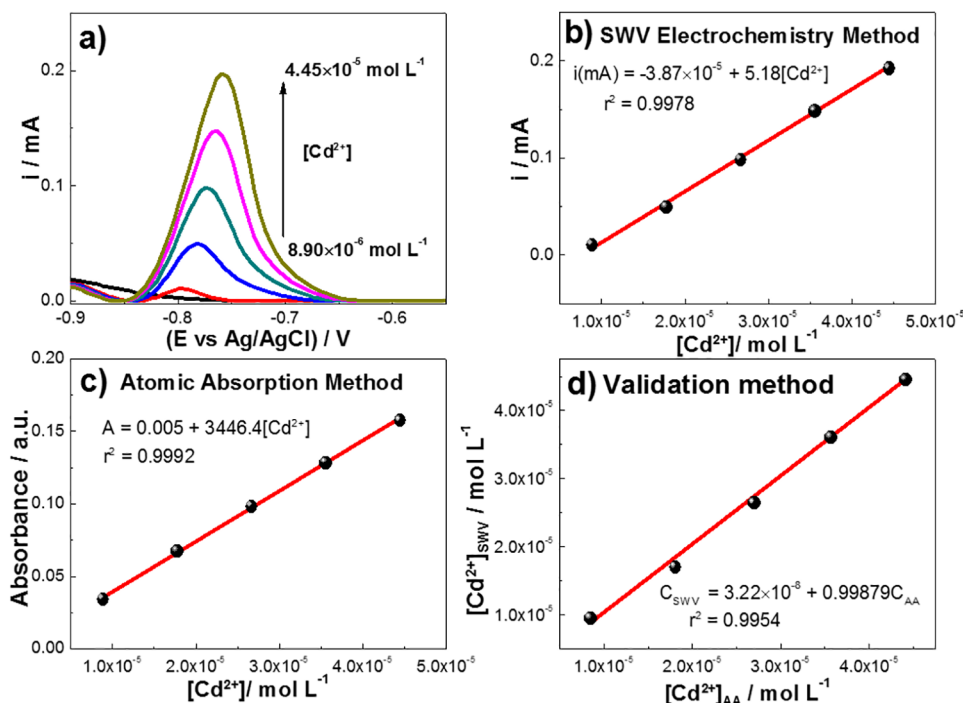
Figure 9. a) SWV analysis of the ACOP/MWCNT−CPE sensor in the presence of Cd^{2+} at 8.90×10^{-6} to 4.45×10^{-5} mol L^{-1} range concentrations in 0.1 mol L^{-1} HCl, (b) calibration curve of the SWV electrochemical method its, (c) calibration curve of the AA method, and (d) validation of the electrochemical method.

quantifying Cd^{2+} concentrations in both synthetic and real samples. To construct the calibration curve for Cd^{2+}, the AA technique was employed within a concentration range of 8.9×10^{-6} to 4.45×10^{-5} mol L^{-1} of Cd^{2+}, mirroring the range employed for the SWV electrochemical technique, as presented in Figure 9 and Table 4. During the electrochemical analysis utilizing the ACOP/MWCNT−CPE sensor and SWV, a strong linear correlation between Δi and $[Cd^{2+}]$ was observed, with an r^2 value of = 0.9978 (see Figure 9a,b). In parallel, the AA analysis generated an analytical curve characterized by a linear relationship and an r^2 value of 0.9992, further attesting to the robust linear correlation between AA and $[Cd^{2+}]$ (see Figure 9c). Subsequently, a correlation was established between the two linear relationships obtained from each technique (AA vs SWV), as depicted in Figure 9d. The equation $[Cd^{2+}]_{SWV} = 3.22 \times 10^{-8} + 0.99879[Cd^{2+}]_{AA}$ ($r^2 = 0.9978$) indicates a good precision and concordance between the SWV electrochemical method and the AA technique. This confirms that the

Table 4. Analysis of Cd^{2+} in Synthetic Samples Using the Electrochemical Method and the Atomic Absorption Method

concentration of Cd^{2+} added (mol L^{-1})	electrochemical method		atomic absorption method	
	Cd^{2+} detected (mol L^{-1})	recovered (%)	Cd^{2+} detected (mol L^{-1})	recovered (%)
8.90×10^{-6}	9.51×10^{-6}	106.91	8.50×10^{-6}	95.49
1.78×10^{-5}	1.70×10^{-5}	95.50	1.81×10^{-5}	101.55
2.67×10^{-5}	2.64×10^{-5}	98.96	2.70×10^{-5}	101.16
3.56×10^{-5}	3.60×10^{-5}	101.25	3.57×10^{-5}	100.35
4.45×10^{-5}	4.45×10^{-5}	100.00	4.42×10^{-5}	99.27

proposed sensor exhibits a reliable electrochemical detection. Finally, the ACOP/MWCNT−CPE sensor was employed for the analysis of real samples extracted from the Rimac River in Lima, Peru. The results are presented in Table 5, showing suitable recovery percentages ranging from 97.33 to 115.6%.

Table 5. Analysis of Cd²⁺ in Real Samples Using the Electrochemical Method and the Atomic Absorption Method

concentration of Cd²⁺ added (mol L⁻¹)	electrochemical method		atomic absorption method	
	Cd²⁺ detected (mol L⁻¹)	recovered (%)	Cd²⁺ detected (mol L⁻¹)	recovered (%)
8.90×10^{-6}	1.02×10^{-5}	115.6	1.02×10^{-5}	115.0
1.78×10^{-5}	1.79×10^{-5}	100.5	1.78×10^{-5}	100.0
2.67×10^{-5}	2.60×10^{-5}	97.33	2.60×10^{-5}	97.33
3.56×10^{-5}	3.59×10^{-5}	100.9	3.59×10^{-5}	101.0
4.45×10^{-5}	4.41×10^{-5}	99.35	4.42×10^{-5}	99.40

CONCLUSIONS

A novel electrochemical sensor was successfully developed to address the critical issue of HM Cd²⁺ in water. The sensor was based on a synergistic combination of AC derived from orange peel (ACOP) and multiwalled carbon nanotubes, resulting in a platform with heightened sensor capabilities. The structural order and functional groups present in the ACOP were characterized using IR and Raman spectroscopy. The ACOP/MWCNT−CPE sensor exhibited remarkable stability and selectivity, displaying robustness against various interferents, including different HMs. In the process of Cd²⁺ detection, the sensor demonstrated a linear working range from 9.09×10^{-6} to 7.29×10^{-5} mol L⁻¹, with $r^2 = 0.9907$. The sensor also achieved a low detection limit of 0.91 ± 0.79 μmol L⁻¹ and a quantification limit of 3.00 ± 2.60 μmol L⁻¹. To validate the performance of the ACOP/MWCNT−CPE sensor, the well-established atomic absorption technique was used, exhibiting excellent correlation. This demonstrates that the sensor serves as an excellent analytical platform for detecting and quantifying Cd²⁺ in both synthetic waters and also with river water samples after acid treatment. This accomplishment signifies a valuable contribution to the field of environmental monitoring and HM detection, opening avenues for future applications and advancements.

ASSOCIATED CONTENT

Ⓢ Supporting Information

The Supporting Information is available free of charge at https://pubs.acs.org/doi/10.1021/acsomega.3c05154.

EDS spectrum of OP and ACOP, analysis of OP and ACOP by nitrogen adsorption−desorption isotherms BET and pore diameter, study of the oxidation current of Cd²⁺ in HCl 0.1 mol L⁻¹, and CV at different scan rates at 0.01−0.3 V s⁻¹ in the presence of Cd²⁺ 9.0×10^{-4} mol L⁻¹ in the electrolyte 0.1 mol L⁻¹ HCl (PDF)

AUTHOR INFORMATION

Corresponding Authors

Angelica M. Baena-Moncada − *Laboratorio de Investigación de Electroquímica of Aplicada, Facultad de Ciencias de la Universidad Nacional de Ingeniería, Lima 51, Peru;* orcid.org/0000-0002-2896-4392; Email: abaenam@uni.edu.pe

Golfer Muedas-Taipe − *Laboratorio de Investigación de Electroquímica de Aplicada, Facultad de Ciencias de la Universidad Nacional de Ingeniería, Lima 51, Peru;* Email: gmuedast@uni.edu.pe

Authors

Luis C. Beas-Bernuy − *Laboratorio de Investigación de Electroquímica of Aplicada, Facultad de Ciencias de la Universidad Nacional de Ingeniería, Lima 51, Peru*

Andy A. Cardenas-Riojas − *Laboratorio de Investigación de Electroquímica of Aplicada, Facultad de Ciencias de la Universidad Nacional de Ingeniería, Lima 51, Peru*

Sandy L. Calderon-Zavaleta − *Laboratorio de Investigación de Electroquímica of Aplicada, Facultad de Ciencias de la Universidad Nacional de Ingeniería, Lima 51, Peru*

Ulises Quiroz-Aguinaga − *Laboratorio de Investigación de Electroquímica of Aplicada, Facultad de Ciencias de la Universidad Nacional de Ingeniería, Lima 51, Peru*

Adolfo La Rosa-Toro − *Laboratorio de Investigación de Electroquímica of Aplicada and Centro para el Desarrollo de Materiales Avanzados y Nanotecnología (CEMAT), Facultad de Ciencias de la Universidad Nacional de Ingeniería, Lima 51, Peru*

Elvis O. López − *Department of Experimental Low Energy Physics, Brazilian Center for Research in Physics (CBPF), Rio de Janeiro 22290-180, Brazil*

Yvan J. O. Asencios − *Institute of Marine Sciences, Federal University of São Paulo (UNIFESP), Sao Paulo 11030-100, Brazil;* orcid.org/0000-0001-6000-9152

Complete contact information is available at:
https://pubs.acs.org/10.1021/acsomega.3c05154

Author Contributions

The manuscript was written through contributions of all authors. /All authors have given approval to the final version of the manuscript.

Notes

The authors declare no competing financial interest.

ACKNOWLEDGMENTS

ABBREVIATIONS

ACOP, orange peel activated carbon; MWCNT, multiwalled carbon nanotube; ACOP/MWCNT, orange peel activated carbon and multiwalled carbon nanotubes composite; CPE, carbon paste electrode; ACOP/MWCNT−CPE, electrochemical sensor; SWV, square wave voltammetry; CV, cyclic voltammetry

REFERENCES

(1) Liu, X.; Yao, Y.; Ying, Y.; Ping, J. Recent Advances in Nanomaterial-Enabled Screen-Printed Electrochemical Sensors for Heavy Metal Detection. *TrAC, Trends Anal. Chem.* **2019**, *115*, 187−202.

(2) Devadas, B.; Sivakumar, M.; Chen, S. M.; Rajkumar, M.; Hu, C. C. Simultaneous and Selective Detection of Environment Hazardous Metals in Water Samples by Using Flower and Christmas Tree Like Cerium Hexacyanoferrate Modified Electrodes. *Electroanalysis* **2015**, *27* (11), 2629−2636.

(3) Duruibe, J. O.; et al. Heavy Metal Pollution and Human Biotoxic Effects. *Int. J. Phys. Sci.* **2007**, *2*, 112.

(4) Li, Y.; Huang, H.; Cui, R.; Wang, D.; Yin, Z.; Wang, D.; Zheng, L.; Zhang, J.; Zhao, Y.; Yuan, H.; Dong, J.; Guo, X.; Sun, B. Electrochemical Sensor Based on Graphdiyne Is Effectively Used to Determine Cd^{2+} and Pb^{2+} in Water. *Sens. Actuators, B* **2021**, *332*, 129519.

(5) Zhou, W.; Li, C.; Sun, C.; Yang, X. Simultaneously Determination of Trace Cd^{2+} and Pb^{2+} Based on L-Cysteine/ Graphene Modified Glassy Carbon Electrode. *Food Chem.* **2016**, *192*, 351−357.

(6) Chiu, T. Y.; Chen, P. H.; Chang, C. L.; Yang, D. M. Live-Cell Dynamic Sensing of Cd^{2+} with a FRET-Based Indicator. *PLoS One* **2013**, *8* (6), No. e65853.

(7) Farzin, L.; Shamsipur, M.; Sheibani, S. A Review: Aptamer-Based Analytical Strategies Using the Nanomaterials for Environmental and Human Monitoring of Toxic Heavy Metals. *Talanta* **2017**, *174*, 619− 627.

(8) Samandari, L.; Bahrami, A.; Shamsipur, M.; Farzin, L.; Hashemi, B. Electrochemical Preconcentration of Ultra-Trace Cd2+ from Environmental and Biological Samples Prior to Its Determination Using Carbon Paste Electrode Impregnated with Ion Imprinted Polymer Nanoparticles. *Int. J. Environ. Anal. Chem.* **2019**, *99* (2), 172−186.

(9) Afzali, D.; Mostafavi, A. Flame Atomic Absorption Spectrometry Determination of Trace Amounts of Ag^+ and Cd^{2+} after Simultaneous Separation and Pre-Concentration on to Modified Clinoptilolite Zeolite as a New Sor-Bent. *Can. J. Anal. Sci. Spect.* **2008**, *53* (2), 82.

(10) de Oliveira, L. L. G.; Suquila, F. A. C.; de Figueiredo, E. C.; Segatelli, M. G.; Tarley, C. R. T. Restricted Access Material-Ion Imprinted Polymer-Based Method for on-Line Flow Preconcentration of Cd^{2+} Prior to Flame Atomic Absorption Spectrometry Determination. *Microchem. J.* **2020**, *157*, 105022.

(11) Zheng, H.; Jia, B.; Zhu, Z.; Tang, Z.; Hu, S. Determination of Trace Amounts of Pb, Cd, Ni and Co by Wavelength-Dispersive X-Ray Fluorescence Spectrometry after Preconcentration with Dithizone Functionalized Graphene. *Anal. Methods* **2014**, *6* (21), 8569−8576.

(12) Vidmar, J.; Oprčkal, P.; Milačič, R.; Mladenovič, A.; Ščančar, J. Investigation of the Behaviour of Zero-Valent Iron Nanoparticles and Their Interactions with Cd2+ in Wastewater by Single Particle ICP-MS. *Sci. Total Environ.* **2018**, *634*, 1259−1268.

(13) Liu, N.; Ye, W.; Liu, G.; Zhao, G. Improving the Accuracy of Stripping Voltammetry Detection of Cd2+ and Pb2+ in the Presence of Cu^{2+} and Zn^{2+} by Machine Learning: Understanding and Inhibiting the Interactive Interference among Multiple Heavy Metals. *Anal. Chim. Acta* **2022**, *1213*, 339956.

(14) Yao, Y.; Wu, H.; Ping, J. Simultaneous Determination of Cd(II) and Pb(II) Ions in Honey and Milk Samples Using a Single-Walled Carbon Nanohorns Modified Screen-Printed Electrochemical Sensor. *Food Chem.* **2019**, *274*, 8−15.

(15) Zhang, C.; Wang, C.; Hao, T.; Lin, H.; Wang, Q.; Wu, Y.; Hu, Y.; Wang, S.; Huang, Y.; Guo, Z. Electrochemical Sensor for the Detection of Ppq-Level Cd^{2+} Based on a Multifunctional Composite Material by Fast Scan Voltammetry. *Sens. Actuators, B* **2021**, *341*, 130037.

(16) Özbek, O.; Isildak, Ö. Polymer-Based Cadmium(II)-Selective Potentiometric Sensors for the Analysis of Cd^{2+} in Different Environmental Samples. *Int. J. Environ. Anal. Chem.* **2021**, *103*, 1587.

(17) Malik, L. A.; Bashir, A.; Qureashi, A.; Pandith, A. H. Detection and Removal of Heavy Metal Ions: A Review. *Environ. Chem. Lett.* **2019**, *17* (4), 1495−1521.

(18) Hamzah, H. H.; Shafiee, S. A.; Abdalla, A.; Patel, B. A. 3D Printable Conductive Materials for the Fabrication of Electrochemical Sensors: A Mini Review. *Electrochem. Commun.* **2018**, *96*, 27−31.

(19) Kokab, T.; Shah, A.; Nisar, J.; Khan, A. M.; Khan, S. B.; Shah, A. H. Tripeptide Derivative-Modified Glassy Carbon Electrode: A Novel Electrochemical Sensor for Sensitive and Selective Detection of Cd^{2+} Ions. *ACS Omega* **2020**, *5* (17), 10123−10132.

(20) Aqlan, F. M.; Alam, M. M.; Al-Bogami, A. S.; Saleh, T. S.; Wani, M. Y.; Al-Farga, A.; Asiri, A. M.; Karim, M. R.; Ahmed, J.; Fazal, M. A.; Rahman, M. M. Efficient Electro-Chemical Sensor for Sensitive Cd2+detection Based on Novel in-Situ Synthesized Hydrazonoyl Bromide (HB). *J. Mol. Struct.* **2021**, *1231*, 129690.

(21) Liu, Y.; Li, T.; Ling, C.; Chen, Z.; Deng, Y.; He, N. Electrochemical Sensor for Cd^{2+} and Pb^{2+} Detection Based on Nano-Porous Pseudo Carbon Paste Electrode. *Chin. Chem. Lett.* **2019**, *30* (12), 2211−2215.

(22) Li, X.; Wen, H.; Fu, Q.; Peng, D.; Yu, J.; Zhang, Q.; Huang, X. Morphology-Dependent NiO Modified Glassy Carbon Electrode Surface for Lead(II) and Cadmium(II) Detection. *Appl. Surf. Sci.* **2016**, *363*, 7−12.

(23) Kokab, T.; Shah, A.; Iftikhar, F. J.; Nisar, J.; Akhter, M. S.; Khan, S. B. Amino Acid-Fabricated Glassy Carbon Electrode for Efficient Simultaneous Sensing of Zinc(II), Cadmium(II), Copper-(II), and Mercury(II) Ions. *ACS Omega* **2019**, *4* (26), 22057−22068.

(24) Hassan, K. M.; Elhaddad, G. M.; AbdelAzzem, M. Voltammetric Determination of Cadmium(II), Lead(II) and Copper-(II) with a Glassy Carbon Electrode Modified with Silver Nano-particles Deposited on Poly(1,8-Diaminonaphthalene). *Microchim. Acta* **2019**, *186* (7), 440−510.

(25) Dahaghin, Z.; Kilmartin, P. A.; Mousavi, H. Z. Determination of Cadmium(II) Using a Glassy Carbon Electrode Modified with a Cd-Ion Imprinted Polymer. *J. Electroanal. Chem.* **2018**, *810*, 185−190.

(26) Xu, Z.; Fan, X.; Ma, Q.; Tang, B.; Lu, Z.; Zhang, J.; Mo, G.; Ye, J.; Ye, J. A Sensitive Electrochemical Sensor for Simultaneous Voltammetric Sensing of Cadmium and Lead Based on Fe3O4/ Multiwalled Carbon Nanotube/Laser Scribed Graphene Composites Functionalized with Chitosan Modified Electrode. *Mater. Chem. Phys.* **2019**, *238*, 121877.

(27) Lochab, A.; Sharma, R.; Kumar, S.; Saxena, R. Recent Advances in Carbon Based Nanomaterials as Electrochemical Sensor for Toxic Metal Ions in Environmental Applications. *Mater. Today: Proc.* **2021**, *45*, 3741−3753.

(28) Sreekanth, S. P.; Alodhayb, A.; Assaifan, A. K.; Alzahrani, K. E.; Muthuramamoorthy, M.; Alkhammash, H. I.; Pandiaraj, S.; Alswieleh, A. M.; Van Le, Q.; Mangaiyarkarasi, R.; Grace, A. N.; Raghavan, V. Multi-Walled Carbon Nanotube-Based Nanobiosensor for the Detection of Cadmium in Water. *Environ. Res.* **2021**, *197*, 111148.

(29) Xu, C.; Liu, J.; Bi, Y.; Ma, C.; Bai, J.; Hu, Z.; Zhou, M. Biomass Derived Worm-like Nitrogen-Doped-Carbon Framework for Trace Determination of Toxic Heavy Metal Lead (II). *Anal. Chim. Acta* **2020**, *1116*, 16−26.

(30) El Hamdouni, Y.; El Hajjaji, S.; Szabó, T.; Trif, L.; Felhősi, I.; Abbi, K.; Labjar, N.; Harmouche, L.; Shaban, A. Biomass Valorization of Walnut Shell into Biochar as a Resource for Electrochemical Simultaneous Detection of Heavy Metal Ions in Water and Soil Samples: Preparation, Characterization, and Applications. *Arabian J. Chem.* **2022**, *15* (11), 104252.

(31) Zhang, X.; Zhang, Y.; Ngo, H. H.; Guo, W.; Wen, H.; Zhang, D.; Li, C.; Qi, L. Characterization and Sulfonamide Antibiotics Adsorption Capacity of Spent Coffee Grounds Based Biochar and Hydrochar. *Sci. Total Environ.* **2020**, *716*, 137015.

(32) Hu, L.; He, Z.; Zhang, S. Sustainable Use of Rice Husk Ash in Cement-Based Materials: Environmental Evaluation and Performance Improvement. *J. Cleaner Prod.* **2020**, *264*, 121744.

(33) Abdel-Shafy, H. I.; Hefny, M.; Ahmed, H. M.; Abdel-Haleem, F. M. Removal of Cadmium, Nickel, and Zinc from Aqueous Solutions by Activated Carbon Prepared from Corncob - Waste Agricultural Materials. *Egypt. J. Chem.* **2022**, *65* (3), 677−687.

(34) Jain, D.; Kanungo, J.; Tripathi, S. K. Enhancement in Performance of Supercapacitor Using Eucalyptus Leaves Derived Activated Carbon Electrode with CH3COONa and HQ Electrolytes:

A Step towards Environment Benign Supercapacitor. *J. Alloys Compd.* **2020**, *832*, 154956.

(35) Bejjanki, D.; Banothu, P.; Kumar, V. B.; Kumar, P. S.; Bejjanki, D.; Banothu, P.; Bhooshan Kumar, V.; Sampath Kumar, P. Biomass-Derived N-Doped Activated Carbon from Eucalyptus Leaves as an Efficient Supercapacitor Electrode Material. *C* **2023**, *9* (1), 24.

(36) Riaz, A.; Lagnika, C.; Abdin, M.; Hashim, M. M.; Ahmed, W. Preparation and Characterization of Chitosan/Gelatin-Based Active Food Packaging Films Containing Apple Peel Nanoparticles. *J. Polym. Environ.* **2020**, *28* (2), 411−420.

(37) Ajay, K. M.; Dinesh, M. N.; Byatarayappa, G.; Radhika, M. G.; Kathyayini, N.; Vijeth, H. Electrochemical Investigations on Low Cost KOH Activated Carbon Derived from Orange-Peel and Polyaniline for Hybrid Supercapacitors. *Inorg. Chem. Commun.* **2021**, *127*, 108523.

(38) Tovar, A. K.; Godínez, L. A.; Espejel, F.; Ramírez-Zamora, R. M.; Robles, I. Optimization of the Integral Valorization Process for Orange Peel Waste Using a Design of Experiments Approach: Production of High-Quality Pectin and Activated Carbon. *Waste Manage.* **2019**, *85*, 202−213.

(39) Peña, K. J.; Giraldo, L.; Moreno, J. C. Preparación de Carbón Activado a Partir de Cáscara de Naranja Por Activación Química. Caracterización Física y Química. *Rev. Colomb. Química* **2012**, *41* (2), 311−323.

(40) Yoon, K.; Cho, D. W.; Bhatnagar, A.; Song, H. Adsorption of As(V) and Ni(II) by Fe-Biochar Composite Fabricated by Co-Pyrolysis of Orange Peel and Red Mud. *Environ. Res.* **2020**, *188*, 109809.

(41) Fernandez, M. E.; Nunell, G. V.; Bonelli, P. R.; Cukierman, A. L. Activated Carbon Developed from Orange Peels: Batch and Dynamic Competitive Adsorption of Basic Dyes. *Ind. Crops Prod.* **2014**, *62*, 437−445.

(42) La Rosa-Toro G, A.; Cardenas Riojas, A. A.; Calderon Zavaleta, S. L.; Quiroz Aguinaga, U.; Muedas Taipe, G.; La Rosa-Toro G, A.; Cardenas Riojas, A. A.; Calderon Zavaleta, S. L.; Quiroz Aguinaga, U.; Muedas Taipe, G. Estudio Electroquímico de La Remoción de Los Iones Cd(II) En Soluciones Acuosas Mediante Carbón Activado Obtenido de La Cáscara de Naranja. *Rev. la Soc. Química del Perú* **2022**, *88* (2), 155−164.

(43) Wan, L.; Chen, D.; Liu, J.; Zhang, Y.; Chen, J.; Du, C.; Xie, M. Facile Preparation of Porous Carbons Derived from Orange Peel via Basic Copper Carbonate Activation for Supercapacitors. *J. Alloys Compd.* **2020**, *823*, 153747.

(44) Arun, S.; Kiran, K. U. V.; Kumar, S. M.; Karnan, M.; Sathish, M.; Mayavan, S. Effect of Orange Peel Derived Activated Carbon as a Negative Additive for Lead-Acid Battery under High Rate Discharge Condition. *J. Energy Storage* **2021**, *34*, 102225.

(45) Espro, C.; Satira, A.; Mauriello, F.; Anajafi, Z.; Moulaee, K.; Iannazzo, D.; Neri, G. Orange Peels-Derived Hydrochar for Chemical Sensing Applications. *Sens. Actuators, B* **2021**, *341*, 130016.

(46) Licona-Aguilar, Á.; Torres-Huerta, A. M.; Domínguez-Crespo, M.; Palma-Ramírez, D.; Conde-Barajas, E.; Negrete-Rodríguez, M.; Rodríguez-Salazar, A.; García-Zaleta, D. Reutilization of Waste Biomass from Sugarcane Bagasse and Orange Peel to Obtain Carbon Foams: Applications in the Metal Ions Removal. *Sci. Total Environ.* **2022**, *831*, 154883.

(47) Wu, W.; Jia, M.; Zhang, Z.; Chen, X.; Zhang, Q.; Zhang, W.; Li, P.; Chen, L. Sensitive, Selective and Simultaneous Electrochemical Detection of Multiple Heavy Metals in Environment and Food Using a Lowcost Fe_3O_4 Nanoparticles/Fluorinated Multi-Walled Carbon Nanotubes Sensor. *Ecotoxicol. Environ. Saf.* **2019**, *175*, 243−250.

(48) Dhelipan, M.; Arunchander, A.; Sahu, A. K.; Kalpana, D. Activated Carbon from Orange Peels as Supercapacitor Electrode and Catalyst Support for Oxygen Reduction Reaction in Proton Exchange Membrane Fuel Cell. *J. Saudi Chem. Soc.* **2017**, *21* (4), 487−494.

(49) Feng, P.; Li, J.; Wang, H.; Xu, Z. Biomass-Based Activated Carbon and Activators: Preparation of Activated Carbon from Corncob by Chemical Activation with Biomass Pyrolysis Liquids. *ACS Omega* **2020**, *5* (37), 24064−24072.

(50) Dollimore, D.; Spooner, P.; Turner, A. The Bet Method of Analysis of Gas Adsorption Data and Its Relevance to the Calculation of Surface Areas. *Surf. Technol.* **1976**, *4* (2), 121−160.

(51) Meng, L.; Zhang, X.; Tang, Y.; Su, K.; Kong, J. Hierarchically Porous Silicon-Carbon-Nitrogen Hybrid Materials towards Highly Efficient and Selective Adsorption of Organic Dyes. *Sci. Rep.* **2015**, *5*, 7910.

(52) Li, F.; Gui, X.; Ji, W.; Zhou, C. Effect of Calcium Dihydrogen Phosphate Addition on Carbon Retention and Stability of Biochars Derived from Cellulose, Hemicellulose, and Lignin. *Chemosphere* **2020**, *251*, 126335.

(53) Turkmen Koc, S. N.; Kipcak, A. S.; Moroydor Derun, E.; Tugrul, N. Removal of Zinc from Wastewater Using Orange, Pineapple and Pomegranate Peels. *Int. J. Environ. Sci. Technol.* **2021**, *18* (9), 2781−2792.

(54) El Nemr, A.; Aboughaly, R. M.; El Sikaily, A.; Ragab, S.; Masoud, M. S.; Ramadan, M. S. Microporous Nano-Activated Carbon Type I Derived from Orange Peel and Its Application for Cr(VI) Removal from Aquatic Environment. *Biomass Convers. Biorefin.* **2022**, *12* (11), 5125−5143.

(55) Gunay Gurer, A.; Aktas, K.; Ozkaleli Akcetin, M.; Erdem Unsar, A.; Asilturk, M. Adsorption Isotherms, Thermodynamics, and Kinetic Modeling of Methylene Blue onto Novel Carbonaceous Adsorbent Derived from Bitter Orange Peels. *Water, Air, Soil Pollut.* **2021**, *232* (4), 138−217.

(56) Thambidurai, A.; Lourdusamy, J. K.; John, J. V.; Ganesan, S. Preparation and Electrochemical Behaviour of Biomass Based Porous Carbons as Electrodes for Supercapacitors - a Comparative Investigation. *Korean J. Chem. Eng.* **2014**, *31* (2), 268−275.

(57) Wei, Q.; Chen, Z.; Cheng, Y.; Wang, X.; Yang, X.; Wang, Z. Preparation and Electrochemical Performance of Orange Peel Based-Activated Carbons Activated by Different Activators. *Colloids Surf., A* **2019**, *574*, 221−227.

(58) Bediako, J. K.; Lin, S.; Sarkar, A. K.; Zhao, Y.; Choi, J. W.; Song, M. H.; Cho, C. W.; Yun, Y. S. Evaluation of Orange Peel-Derived Activated Carbons for Treatment of Dye-Contaminated Wastewater Tailings. *Environ. Sci. Pollut. Res.* **2020**, *27* (1), 1053−1068.

(59) Kallem, P.; Ouda, M.; Bharath, G.; Hasan, S. W.; Banat, F. Enhanced Water Permeability and Fouling Resistance Properties of Ultrafiltration Membranes Incorporated with Hydroxyapatite Decorated Orange-Peel-Derived Activated Carbon Nanocomposites. *Chemosphere* **2022**, *286*, 131799.

(60) Shu, J.; Cheng, S.; Xia, H.; Zhang, L.; Peng, J.; Li, C.; Zhang, S. Copper Loaded on Activated Carbon as an Efficient Adsorbent for Removal of Methylene Blue. *RSC Adv.* **2017**, *7* (24), 14395−14405.

(61) Li, Z.; Deng, L.; Kinloch, I. A.; Young, R. J. Raman Spectroscopy of Carbon Materials and Their Composites: Graphene, Nanotubes and Fibres. *Prog. Mater. Sci.* **2023**, *135*, 101089.

(62) Murphy, H.; Papakonstantinou, P.; Okpalugo, T. I. T. Raman Study of Multiwalled Carbon Nanotubes Functionalized with Oxygen Groups. *J. Vac. Sci. Technol., B: Microelectron. Nanometer Struct.– Process., Meas., Phenom.* **2006**, *24* (2), 715−720.

(63) Obraztsova, E. D.; Fujii, M.; Hayashi, S.; Kuznetsov, V. L.; Butenko, Y. V.; Chuvilin, A. L. Raman Identification of Onion-like Carbon. *Carbon* **1998**, *36* (5–6), 821−826.

(64) Dresselhaus, M. S.; Dresselhaus, G.; Saito, R.; Jorio, A. Raman Spectroscopy of Carbon Nanotubes. *Phys. Rep.* **2005**, *409* (2), 47−99.

(65) Dresselhaus, M. S.; Jorio, A.; Hofmann, M.; Dresselhaus, G.; Saito, R. Perspectives on Carbon Nanotubes and Graphene Raman Spectroscopy. *Nano Lett.* **2010**, *10* (3), 751−758.

(66) El-Hendawy, A. N. A. Variation in the FTIR Spectra of a Biomass under Impregnation, Carbonization and Oxidation Conditions. *J. Anal. Appl. Pyrolysis* **2006**, *75* (2), 159−166.

(67) Ramutshatsha-Makhwedzha, D.; Mavhungu, A.; Moropeng, M. L.; Mbaya, R. Activated Carbon Derived from Waste Orange and Lemon Peels for the Adsorption of Methyl Orange and Methylene Blue Dyes from Wastewater. *Heliyon* **2022**, *8* (8), No. e09930.

(68) Yang, H.; Yan, R.; Chen, H.; Lee, D. H.; Zheng, C. Characteristics of Hemicellulose, Cellulose and Lignin Pyrolysis. *Fuel* **2007**, *86* (12−13), 1781−1788.

(69) Xing, H.; Xu, J.; Zhu, X.; Duan, X.; Lu, L.; Wang, W.; Zhang, Y.; Yang, T. Highly Sensitive Simultaneous Determination of Cadmium (II), Lead (II), Copper (II), and Mercury (II) Ions on N-Doped Graphene Modified Electrode. *J. Electroanal. Chem.* **2016**, *760*, 52−58.

(70) Lakshmana Naik, R.; Rupas Kumar, M.; Bala Narsaiah, T. Removal of Heavy Metals (Cu & Ni) from Wastewater Using Rice Husk and Orange Peel as Adsorbents. *Mater. Today: Proc.* **2023**, *72*, 92−98.

(71) Ascencio-Flores, Y. F.; Carhuayal-Alvarez, S. M.; Quiroz-Aguinaga, U.; Calderon-Zavaleta, S. L.; López, E. O.; Ponce-Vargas, M.; Cardenas-Riojas, A. A.; Baena-Moncada, A. M. Simultaneous Square Wave Voltammetry Detection of Azo Dyes Using Silver Nanoparticles Assembled on Carbon Nanofibers. *Electrochim. Acta* **2023**, *441*, 141782.

(72) Cardenas-Riojas, A. A.; Calderon-Zavaleta, S. L.; Quiroz-Aguinaga, U.; López, E. O.; Ponce-Vargas, M.; Baena-Moncada, A. M. Evaluation of an Electrochemical Sensor Based on Gold Nanoparticles Supported on Carbon Nanofibers for Detection of Tartrazine Dye. *J. Solid State Electrochem.* **2023**, *27*, 1969−1982.

(73) Palanna, M.; Aralekallu, S.; Keshavananda Prabhu, C. P.; Sajjan, V. A.; Mounesh; Sannegowda, L. K.; Sannegowda, L. K. Nanomolar Detection of Mercury(II) Using Electropolymerized Phthalocyanine Film. *Electrochim. Acta* **2021**, *367*, 137519.

(74) Sajjan, V. A.; Aralekallu, S.; Nemakal, M.; Palanna, M.; Prabhu, C. K.; Sannegowda, L. K. Nanomolar Detection of Lead Using Electrochemical Methods Based on a Novel Phthalocyanine. *Inorg. Chim. Acta* **2020**, *506*, 119564.

(75) Aralekallu, S.; Palanna, M.; Hadimani, S.; Prabhu C P, K.; Sajjan, V. A.; Thotiyl, M. O.; Sannegowda, L. K. Biologically Inspired Catalyst for Electrochemical Reduction of Hazardous Hexavalent Chromium. *Dalton Trans.* **2020**, *49* (42), 15061−15071.

(76) Dianat, S.; Hatefi-Mehrjardi, A.; Mahmoodzadeh, K.; Kakhki, S. Electrocatalytic Determination of Cd^{2+} and Pb2+ Using an L-Cysteine Tungstophosphate Self-Assembled Monolayer on a Polycrystalline Gold Electrode. *New J. Chem.* **2019**, *43* (36), 14417−14425.

(77) Ding, S.; Ali, A.; Jamal, R.; Xiang, L.; Zhong, Z.; Abdiryim, T. An Electrochemical Sensor of Poly(EDOT-Pyridine-EDOT)/Graphitic Carbon Nitride Composite for Simultaneous Detection of Cd^{2+} and Pb^{2+}. *Materials* **2018**, *11* (5), 702.

(78) Zhu, X.; Liu, B.; Chen, S.; Wu, L.; Yang, J.; Liang, S.; Xiao, K.; Hu, J.; Hou, H. Ultrasensitive and Simultaneous Electrochemical Determination of Pb^{2+} and Cd^{2+} Based on Biomass Derived Lotus Root-Like Hierarchical Porous Carbon/Bismuth Composite. *J. Electrochem. Soc.* **2020**, *167* (8), 087505.

(79) Djebbi, M. A.; Allagui, L.; El Ayachi, M. S.; Boubakri, S.; Jaffrezic-Renault, N.; Namour, P.; Ben Haj Amara, A. Zero-Valent Iron Nanoparticles Supported on Biomass-Derived Porous Carbon for Simultaneous Detection of Cd^{2+} and Pb2+. *ACS Appl. Nano Mater.* **2022**, *5* (1), 546−558.

(80) Carhuayal-Alvarez, S. M.; Ascencio-Flores, Y. F.; Quiroz-Aguinaga, U.; Calderon-Zavaleta, S. L.; Muedas-Taipe, G.; Cardenas-Riojas, A. A.; Ponce-Vargas, M.; Baena-Moncada, A. M. Square-Wave Voltammetric Detection of Zn(II) and Cd(II) with a Graphite/Carbon Paste Electrode Decorated with 2-Hydroxy-1,4-naphthoquinone. *ACS ES&T Water* **2023**, *3* (8), 2604−2615.